

# Evaluating the Effectiveness of Hybrid Quantum-Classical Convolutional Neural Networks for Image Classification in Multiple Color Spaces

Kwok-Ho Ng  
 College of Cyber Security  
 Jinan University, China  
 kwokhong@stu2024.jnu.edu.cn

Tingting Song  
 College of Cyber Security  
 Jinan University, China  
 tingtingsong@jnu.edu.cn

## Abstract

*As the complexity and scale of image processing tasks continue to expand, quantum convolutional neural networks (QCNNs) have demonstrated the capability to improve image processing performance. These networks can accelerate processing speed and enhance classification accuracy while reducing the number of model parameters. However, these studies restrict images to the RGB color space, and the effectiveness of QCNNs in other color spaces still needs to be explored. In this work, we propose a hybrid quantum-classical convolutional neural network (HQCCNN) model to analyze performance in four different color space images: RGB, Lab, YCrCb, and HSV. Using several multi-qubit entangled gates, HQCCNN is constructed as a parameterized quantum circuit model to evaluate classification performance across these color spaces. Furthermore, we verify the effectiveness of HQCCNN on the CIFAR-100 dataset. The experimental results show that it achieves significantly greater accuracy in binary classification tasks within the RGB color space. For some superclasses, the model performs in the Lab, YCrCb, and HSV color spaces as well as or better than RGB. This serves as an essential reference for QCNN in processing various color space image data for computer vision applications.*

Convolutional neural networks (CNNs) have been widely applied to computer vision tasks and have achieved remarkable success, especially in image recognition tasks [33, 44]. The hierarchical structure of CNNs is designed to extract features from images efficiently. With the increasing scale of models and the introduction of innovative designs, such as ResNet [12] and DenseNet [14], CNNs continue to be among the most dominant algorithms in image classification today.

However, classical algorithms face significant computational resource challenges when dealing with high-dimensional data, and these computational bottlenecks become even more apparent in more complex tasks. With the rapid development of quantum information and quantum computing, quantum computing is believed to have the potential for exponential speedups [1, 7, 16], which could significantly enhance performance in computer vision and other tasks that require high-dimensional data processing. Furthermore, quantum neural networks (QNNs), a type of quantum algorithm, are being actively studied and developed to explore how quantum computing could be integrated with classical machine learning models to achieve potential quantum advantages [37]. Gil-Fuster et al. [11] demonstrated that quantum machine learning could potentially achieve good generalization with only a small amount of training data.

Quantum convolutional neural networks (QCNNs) are quantum algorithms inspired by classical CNNs. Their structure, similar to that of classical CNN, was proposed by Cong et al. [8]. QCNN consists of convolutional layers, pooling layers, and fully connected layers, designed to extract features and process information from quantum states. By integrating the layered architecture of classical convolutional network with the high-dimensional properties of quantum computation, QCNN demonstrate significant advantages in handling complex data. In particular, QCNN can efficiently utilize a small number of variational parameters to achieve effective training, which makes them highly promising for feature extraction and classification in

## 1. Introduction

Computer image classification is one of the core research areas in computer vision. It finds extensive applications across various domains, such as object classification in autonomous driving [9, 43], disease classification from computed tomography images [31, 42] in the medical field, defect detection in the industrial sector [34, 40], and product identification and classification in agriculture [27, 47]. As the accuracy of image classification continues to improve and algorithms advance, it drives rapid and efficient progress across these domains.

image processing tasks [11]. Furthermore, the QCNN architecture has been shown to exhibit an absence of barren plateaus [30], setting it apart from other QNNs due to its ability to be trainable even with random initialization. This feature ensures that QCNNs can be effectively optimized without encountering the vanishing gradient problem that commonly affects other quantum models.

Currently, the application of QCNN in image classification tasks has primarily focused on single-channel image datasets, such as MNIST. QCNN has demonstrated excellent performance on these datasets, achieving high classification accuracy while significantly reducing the number of parameters compared to classical models [38]. Despite the success of QCNN in single-channel image classification tasks, its application to color image datasets remains limited, with most studies focusing primarily on the RGB color space, while exploration in other color spaces, such as Lab, YCrCb, and HSV, remains relatively insufficient.

In classical CNN research, different color spaces have been extensively explored. For instance, the Lab color space has shown superior performance in plant pest identification tasks [18]; the YCrCb color space outperformed RGB in image forgery detection tasks [32]; and in the context of automated tomato harvesting in complex environments, the HSV color model enabled more accurate identification of tomato ripeness [24]. Therefore, studying different color spaces is crucial for enhancing model robustness and generalization capabilities. Further exploration of QCNN in these color spaces could provide valuable insights into its performance across different color characteristics and its potential advantages in diverse image datasets.

To explore the potential advantages of QCNN in these color spaces, we propose a hybrid quantum-classical convolutional neural network (HQCCNN) model, as shown in Figure 2. HQCCNN combines the strengths of quantum computing with classical neural networks, where the quantum part is responsible for extracting complex features, and the classical part performs fully connected layer operations and loss calculation to enhance classification performance. We first downscale the CIFAR-100 dataset images and then convert them into different color spaces, including Lab, YCrCb, and HSV, as shown in Figure 1. Each image is processed with a fixed convolutional kernel size of (2, 2), with four pixel values from each channel being encoded into quantum states. After the encoding, parameterized quantum circuits (PQCs) evolve the quantum bits, followed by measurement to obtain feature values corresponding to the three channels.

The main contributions in our work: **(1)** Our HQCCNN model demonstrates classification accuracy across different color spaces, offering a novel perspective on leveraging quantum advantages in computer vision. This advantage has not been sufficiently explored in existing quantum com-

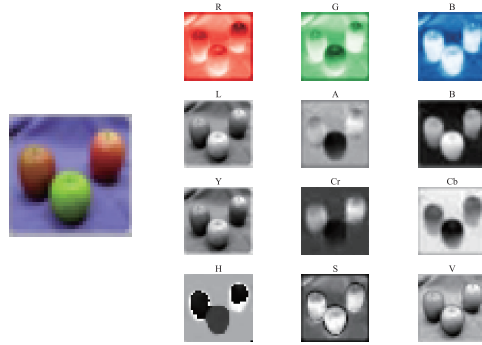


Figure 1. Plotted each channel of the image in four color spaces (RGB, Lab, YCrCb, and HSV).

puting research, so our study provides an important contribution to the field. **(2)** Furthermore, we optimized the conventional QCNN by reducing the number of multi-qubit gates in the first layer. After encoding and applying parameterized gates to each color channel, the initial entanglement operation between channels is designed as an optional module to assess its impact on model performance. This flexibility helps to explore the role of different quantum structures in specific tasks and offers new insights for designing quantum computing models.

The remainder of this paper is organized as follows: Section 2 provides an overview of the current applications of HQCCNN in image classification tasks. Section 3 presents the detailed composition and implementation of the proposed HQCCNN model. Section 4 reports the experimental results of binary classification tasks across different color spaces. Finally, Section 5 summarizes our work and discusses future research directions.

## 2. Related work

In this section, we provide a brief introduction to PQCs, along with a discussion of recent advancements related to the HQCCNN model in the context of color image classification.

Currently, we are in the noisy intermediate-scale quantum (NISQ) era, where quantum hardware is affected by noise. Therefore, designing effective quantum algorithms that can operate on such noisy devices is critical. PQC offers a concrete solution for this requirement [3]. It has been utilized to develop various quantum algorithms, such as the variational quantum eigensolver (VQE) [29] and the quantum approximate optimization algorithm (QAOA) [10]. These algorithms have shown promise in practical applications, including electronic structure research [17] and solving the MaxCut optimization problem [45].

Due to its high flexibility, PQC has become an ideal choice for exploring quantum advantages on NISQ devices.

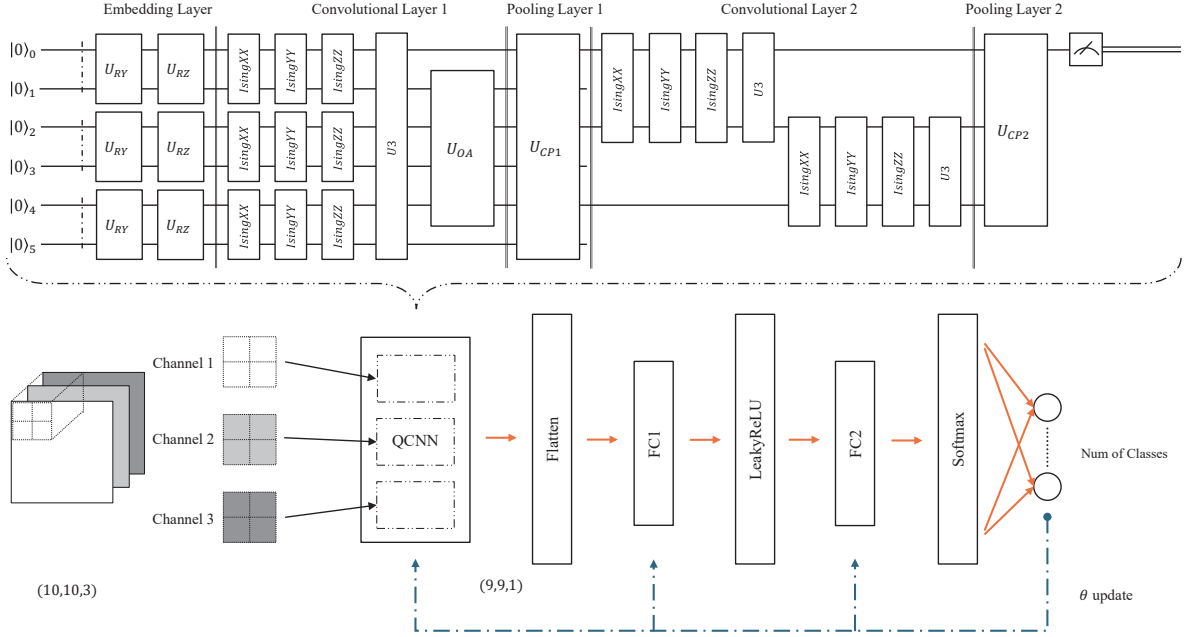


Figure 2. Details of our proposed the HQCCNN model, shows the main components of the QCNN, as well as the overall image processing workflow. This includes the relationship between image channel encoding and qubit positions within the QCNN, and the output feature map size of the quantum layer.

It can approach the target value of specific tasks by adjusting variational parameters. The QCNN model takes full advantage of this flexibility, demonstrating outstanding performance in certain quantum computing tasks. Building on this foundation, HQCCNN further integrates the robustness of classical algorithms, making the final classification results more reliable and stable.

In the early work proposed by Henderson *et al.* [13], their QCNN was compared with CNN and a random model on the MNIST dataset for classification accuracy. The experimental results demonstrated that, compared to CNN, the proposed QCNN became more accurate as the number of training iterations increased, and adding a certain number of quantum filters further improved the model performance. In deeper hybrid classical models, the inclusion of quantum convolutional layers improved the network’s accuracy. Ovalle-Magallanes *et al.* [25] showed that, for the MNIST classification task, ablation experiments on the QCNN model revealed that increasing the size and number of convolutional kernels in the PQC does not always lead to optimal classification accuracy. Liu *et al.* [21] proposed an HQCCNN, which is one of the earliest hybrid models applied to image classification tasks. This model uses a global phase measurement method to measure all qubits and generate multi-channel feature maps. The classification results

on the Tetris dataset indicate that it could even surpass the accuracy of classical CNN.

Jing *et al.* [15] proposed two quantum convolutional circuits that compare different methods for extracting inter-channel and intra-channel information. Experimental results show that these newly proposed quantum convolutional circuits achieve higher test accuracy than classical CNN in RGB image classification tasks. Moreover, their work demonstrates that the design of larger PQCs can improve the performance of multi-class classification tasks.

Riaz *et al.* [35] proposed a QCNN model without parameter updates, which showed better performance than QCNN with randomly generated PQCs on the MNIST and CIFAR-10 datasets. However, its accuracy declined on the german traffic sign recognition benchmark (GTSRB) dataset, suggesting that the application of quantum algorithm-based classifiers still requires further investigation for colored and complex datasets. Smaldone *et al.* [41] proposed a QCNN for multi-channel image processing, which achieved higher accuracy on the CIFAR-10 dataset compared to previous work [15], despite having reduced quantum circuit complexity.

Yang and Sun [48] proposed a hybrid quantum-classical model for detecting defects in semiconductor wafers. They conducted an ablation study on several PQCs [39]. Ex-

perimental results showed that angle embedding achieved higher accuracy compared to basis state encoding and amplitude encoding, and circuits with better entangling and expressive capabilities demonstrated significant advantages. Under conditions of limited quantum resources, the hybrid quantum model achieved the highest accuracy compared to classical CNN models on the LIT hotspot (ICCAD-2012) and defect wafer map (WM-811K) datasets. Senokosov et al. [38] proposed two types of hybrid neural networks. The first model parallelizes quantum circuits, achieving classification accuracy exceeding 99% on the MNIST and Medical MNIST datasets and over 82% on the CIFAR-10 dataset, with eight times fewer parameters than classical models. The second model incorporates quantum convolutional layers, performing similarly to classical models but with four times fewer parameters.

Currently, research on QCNN for color image classification has primarily focused on the RGB color space, while in more general scenarios, studies have mostly concentrated on grayscale image processing [19]. However, QCNN or hybrid quantum-classical models remain relatively limited for image classification in other color spaces.

### 3. Method

Our HQCCNN model consists of quantum and classical layers. In the quantum layer, classical image information is first encoded as quantum states, leveraging quantum computation to exploit the advantages of operating within a high-dimensional Hilbert space. After evolving through the PQC, we apply local measurements on the quantum bits to avoid vanishing gradients caused by the barren plateau problem [6], thereby extracting the image features. Our method doesn't require additional preprocessing of image data through classical neural networks, and allows quantum computing to be directly applied to the raw data input. Furthermore, the design of the quantum layer is inspired by the construction of the quantum circuit demonstrated by Kottmann et al. [20] in the PennyLane documentation.

#### 3.1. Quantum layer

The quantum layer we designed consists of three main blocks: the embedding, convolutional, and pooling layers. This design follows the quantum circuit structure proposed by Barenco et al. [2] in their work, and is computed sequentially from left to right.

##### 3.1.1. Embedding layer

In the quantum embedding layer, we use parameterized rotation gates  $RY$  and  $RZ$  for encoding. These two single-qubit gates can be described by Equation (1) and Equation (2), respectively.

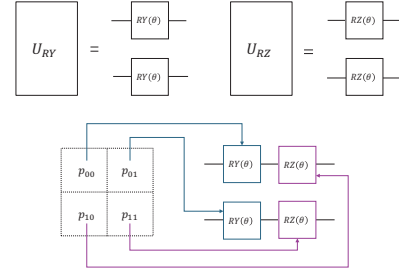


Figure 3. Quantum encoding is performed using two unitary operators, composed of controlled rotation gates  $RY$  and  $RZ$ , respectively. The four pixels are sequentially encoded into corresponding rotation gates at specific positions.

$$RY(\theta) = e^{-i\theta\sigma_y/2} = \begin{bmatrix} \cos(\theta/2) & -\sin(\theta/2) \\ \sin(\theta/2) & \cos(\theta/2) \end{bmatrix} \quad (1)$$

$$RZ(\theta) = e^{-i\theta\sigma_z/2} = \begin{bmatrix} e^{-i\theta/2} & 0 \\ 0 & e^{i\theta/2} \end{bmatrix} \quad (2)$$

The corresponding unitary operators  $U_{RY}$  and  $U_{RZ}$  are illustrated as shown in Figure 3. The four pixel values extracted by the convolution kernel are encoded into quantum states using angle embedding via the  $RY$  gate, where the angle  $\theta$  is embedded. Similarly, the remaining two values are further encoded using the  $RZ$  gate.

##### 3.1.2. Convolutional layer

After encoding, the convolutional operation uses three different parameterized two-qubit operators: IsingXX, IsingYY, and IsingZZ. Each operator is implemented with two  $CNOT$  gates for entanglement and a parameterized rotation gate, as shown in Figure 5.

The mathematical representation of the  $CNOT$  gate, which is commonly used to entangle different qubits, is shown in Equation (3).

$$CNOT = \begin{bmatrix} 1 & 0 & 0 & 0 \\ 0 & 1 & 0 & 0 \\ 0 & 0 & 0 & 1 \\ 0 & 0 & 1 & 0 \end{bmatrix} \quad (3)$$

In the IsingXX (IsingYY or IsingZZ) two-qubit gate, the parameterized rotation gate,  $RX$  ( $RY$  or  $RZ$ ) gate, is represented by Equation (4) (Equation (1) or Equation (2)).

$$RX(\theta) = e^{-i\theta\sigma_x/2} = \begin{bmatrix} \cos(\theta/2) & -i\sin(\theta/2) \\ -i\sin(\theta/2) & \cos(\theta/2) \end{bmatrix} \quad (4)$$

These unitary operators further enhance the representation of pixel information encoded in quantum states within

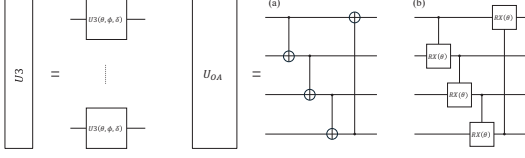


Figure 4. The unitary block  $U3$  consists of independently applying a single-qubit parameterized gate  $U3$  to each qubit. And  $U_{OA}$ (a) performs full connectivity using  $CNOT$  gates, while  $U_{OA}$ (b) achieves full connectivity using the controlled rotation parameterized gate  $CRX$ .

the high-dimensional Hilbert space. Subsequently, each qubit is operated by an independent single-qubit unitary operator  $U3$ , which has three trainable parameters  $(\theta, \phi, \delta)$ , as shown in Figure 4.

$$U3(\theta, \phi, \delta) = \begin{bmatrix} \cos(\theta/2) & -e^{i\delta} \sin(\theta/2) \\ e^{i\phi} \sin(\theta/2) & e^{i(\phi+\delta)} \cos(\theta/2) \end{bmatrix} \quad (5)$$

Furthermore, we design an optional addition fully connected unitary operator  $U_{OA}$ , which can be omitted, leading directly to the pooling layer  $U_{CP1}$  for the next computation. The two additional options are shown in Figure 4. Option  $U_{OA}$ (a) uses  $CNOT$  gates to create a full linear connection among the four-qubit, while option  $U_{OA}$ (b) uses controlled rotation gates  $CRX$  in Equation (6) to fully connect the three color channels of the image. The choice of controlled X-rotation gates is motivated by the findings of Sim et al. [39], who demonstrated that the  $CRX$  gate outperforms the  $CRZ$  gate in terms of expressibility and entangling capability.

$$CRX(\theta) = \begin{bmatrix} 1 & 0 & 0 & 0 \\ 0 & 1 & 0 & 0 \\ 0 & 0 & \cos(\theta/2) & -i \sin(\theta/2) \\ 0 & 0 & -i \sin(\theta/2) & \cos(\theta/2) \end{bmatrix} \quad (6)$$

### 3.1.3. Pooling layer

The pooling layer is used to extract key information from each channel. Two structures of the pooling layer are shown in Figure 5, both implemented using two-qubit controlled phase shift (CP) gates, and the  $CP$  gate can be described mathematically as shown in Equation (7). Similarly to the pooling layer in classical CNN, the quantum pooling layer  $U_{CP1}$  extracts quantum features of the image and reduces

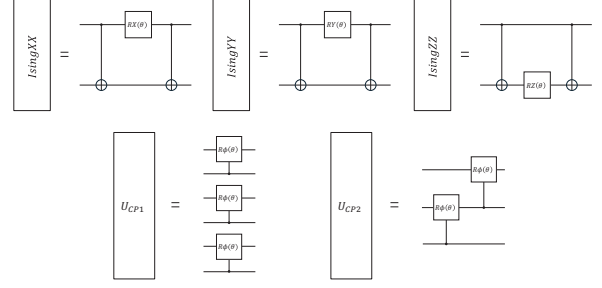


Figure 5. The decomposition of the two-qubit Ising parameterized gate, and the quantum pooling layer is implemented using controlled phase gates applied at two distinct positions.

the number of qubits entering the next quantum convolutional layer. The second pooling layer  $U_{CP2}$  further refines the feature extraction process using trainable parameters while simultaneously performing a simplified, fully connected operation to replace complex quantum algorithms, thereby reducing the number of parameters and computational resources.

$$CP(\theta) = CR_\phi(\theta) = \begin{bmatrix} 1 & 0 & 0 & 0 \\ 0 & 1 & 0 & 0 \\ 0 & 0 & 1 & 0 \\ 0 & 0 & 0 & e^{i\theta} \end{bmatrix} \quad (7)$$

## 3.2. Classical layer

The classical layer of our proposed HQCCNN model consists mainly of fully connected layers and classical optimization algorithms.

After being processed by the QCNN, each image generates a feature map, is flattened, and passed to the first fully connected layer to extract important features further. For the activation function, we utilize the leaky rectified linear unit (LeakyReLU) [23] to ensure effective backpropagation even when negative inputs are present. The results are then passed on to the second fully connected layer (FC2), with an output size determined by the number of classes in the current classification task. The output values are then converted into a probability distribution by applying the Softmax function [46]. Finally, the cross-entropy loss function [36] calculates the error between the predicted results and the true labels, and this error is backpropagated to compute and update the parameters of both the quantum and classical layers.

## 4. Results

First, we preprocessed the CIFAR-100 dataset by resizing the image dimensions from  $(32, 32, 3)$  to  $(10, 10, 3)$  using



	Fish	Flowers	Fruit	Insects	Carnivores	Scenes	People	Trees	Vehicles1	Vehicles2
R*[0, 1]	<b>0.8303</b>	<b>0.8482</b>	<b>0.8794</b>	0.7678	<b>0.7633</b>	<b>0.8303</b>	0.6071	0.7410	<u>0.7901</u>	0.8258
L*[0, 1]	<b>0.8258</b>	0.6919	<b>0.8303</b>	0.7500	<b>0.7946</b>	0.8035	<u>0.6294</u>	0.7232	0.7812	0.8526
Y*[0, 1]	<b>0.7991</b>	0.6607	0.8348	<u>0.7812</u>	<b>0.7991</b>	<b>0.8392</b>	0.5491	<u>0.7500</u>	0.7589	<b>0.8526</b>
H*[0, 1]	0.6830	0.7857	0.8616	0.7053	0.6562	0.7901	0.6116	<b>0.6964</b>	0.7142	<b>0.8616</b>
R*[1, 2]	0.7366	<u>0.6741</u>	0.8794	0.7857	0.5892	0.8258	0.5669	<b>0.8080</b>	<b>0.8437</b>	<b>0.8348</b>
L*[1, 2]	<u>0.7544</u>	<u>0.5758</u>	0.8035	0.7812	<u>0.6830</u>	<b>0.8080</b>	0.5803	<b>0.8437</b>	<b>0.8035</b>	<b>0.8616</b>
Y*[1, 2]	0.7098	0.5580	<b>0.8883</b>	<u>0.7901</u>	0.6696	0.8035	0.6071	<b>0.7857</b>	<b>0.8392</b>	0.7991
H*[1, 2]	0.7500	0.6562	<b>0.8928</b>	0.6785	0.6696	<b>0.8437</b>	<u>0.6160</u>	0.6785	0.6696	0.8571
R*[2, 3]	0.7366	0.7455	<u>0.7991</u>	0.6383	0.6651	0.7946	<b>0.6741</b>	0.6919	<u>0.8214</u>	0.7544
L*[2, 3]	<u>0.7455</u>	0.7053	0.7276	0.6339	0.6696	0.7455	<b>0.7053</b>	<u>0.7410</u>	0.7901	0.7321
Y*[2, 3]	0.7321	<b>0.7767</b>	0.7723	<u>0.6919</u>	<u>0.7410</u>	0.8035	<b>0.7321</b>	0.6919	0.7544	<u>0.7723</u>
H*[2, 3]	0.6830	<b>0.8437</b>	0.7901	0.6607	0.6919	<u>0.8348</u>	<b>0.6294</b>	0.6339	<b>0.7410</b>	0.6964
R*[3, 4]	<u>0.8348</u>	0.7187	0.6785	<b>0.9017</b>	<u>0.7500</u>	0.6830	0.6116	0.6919	0.7366	0.7232
L*[3, 4]	0.7767	<b>0.7410</b>	0.6562	<b>0.9241</b>	0.6875	0.6785	0.5937	0.6607	<u>0.7410</u>	0.6964
Y*[3, 4]	0.7366	0.7276	0.7053	<b>0.9196</b>	0.7142	0.7857	0.5446	<u>0.6964</u>	0.6875	<u>0.7723</u>
H*[3, 4]	<b>0.7946</b>	0.7410	<u>0.7098</u>	<b>0.8526</b>	<b>0.7142</b>	<u>0.7991</u>	<u>0.6160</u>	0.6562	0.6428	0.7366

Table 1. In our minimally designed PQC in hybrid model, we evaluated the performance of binary classification tasks on subclasses of ten superclasses from the CIFAR-100 dataset. Bold indicates the highest accuracy obtained in a particular color space for a given subclass within a superclass, which helps determine which color space performs better. Underline indicates the color space that achieved the highest accuracy across the same binary classification dataset. Here, R\*, L\*, Y\* and H\* are abbreviations for RGB, Lab, YCrCb, and HSV, respectively.

	Fish		Fruit		Insects		Scenes		Vehicles2	
	<i>CNOT</i>	<i>CRX</i>	<i>CNOT</i>	<i>CRX</i>	<i>CNOT</i>	<i>CRX</i>	<i>CNOT</i>	<i>CRX</i>	<i>CNOT</i>	<i>CRX</i>
R*[0, 1]	<b>0.8169</b>	<b>0.8348</b>	<b>0.9330</b>	<b>0.9107</b>	0.7366	<b>0.7767</b>	<b>0.8482</b>	<b>0.8526</b>	0.8258	0.8348
L*[0, 1]	0.7857	0.8169	0.8169	0.8125	0.7276	0.6651	0.8035	0.7946	<b>0.8303</b>	<b>0.8660</b>
Y*[0, 1]	0.8035	0.8035	0.8616	0.8035	0.7589	0.7633	0.8437	0.8169	0.8214	<b>0.8660</b>
H*[0, 1]	0.7053	0.7187	0.8616	0.8750	<b>0.7678</b>	0.7276	0.8258	0.8169	0.8258	0.8571
R*[1, 2]	<b>0.7276</b>	<b>0.7901</b>	<b>0.9464</b>	<b>0.9330</b>	0.7857	<b>0.7946</b>	<b>0.8750</b>	<b>0.8794</b>	0.8839	0.8348
L*[1, 2]	<b>0.7276</b>	0.7232	0.8750	0.8928	0.7321	0.7544	0.8125	0.7767	0.8348	<b>0.8526</b>
Y*[1, 2]	0.6830	0.7321	0.8750	0.8794	<b>0.7991</b>	0.7900	0.8169	0.8392	<b>0.8883</b>	0.8482
H*[1, 2]	0.7232	0.7410	0.8928	<b>0.9330</b>	0.7276	0.7053	0.8303	0.8482	0.8035	0.7901
R*[2, 3]	<b>0.7991</b>	0.7053	<b>0.8125</b>	<b>0.8482</b>	0.6383	0.6562	0.8080	<b>0.8348</b>	0.7142	0.7276
L*[2, 3]	0.7276	0.7410	0.7946	0.7767	<b>0.6428</b>	0.6562	<b>0.8437</b>	0.7410	0.7187	0.7232
Y*[2, 3]	0.5625	<b>0.8187</b>	0.7455	0.7544	0.6160	0.6473	0.7723	0.7946	<b>0.7455</b>	<b>0.7678</b>
H*[2, 3]	0.7276	0.6875	0.7812	0.7991	0.6785	<b>0.7098</b>	0.7901	0.8169	0.6294	0.6964
R*[3, 4]	<b>0.8214</b>	<b>0.8169</b>	<b>0.7812</b>	<b>0.7812</b>	<b>0.9285</b>	<b>0.9151</b>	0.7901	0.7366	0.7008	0.7053
L*[3, 4]	0.7633	0.7767	0.6250	0.7053	0.9062	0.8928	<b>0.8214</b>	0.6741	0.7187	0.7142
Y*[3, 4]	0.7857	0.7678	0.5758	0.6562	0.8928	<b>0.9151</b>	0.7946	0.7901	0.7187	0.7008
H*[3, 4]	0.7767	0.7767	0.7276	0.7098	0.8571	0.8928	0.7991	<b>0.8214</b>	<b>0.7500</b>	<b>0.7857</b>

Table 2. We conducted ablation studies on the selected five superclasses. In our proposed HQCCNN model, the classification accuracies were obtained under different  $U_{OA}$  configurations and color spaces.

bilinear interpolation. Then, we used the functions provided by OpenCV [5] to convert the RGB images into Lab,

YCrCb, and HSV color spaces. Subsequently, all the image data were scaled in the range of  $[0, \pi]$  using MinMaxScaler

from scikit-learn [28].

The quantum convolutional kernel size (2, 2) and operated on all three channels of the image, with a sliding window  $stride = 1$ . During training, we used the AdamW optimizer[22] to update model parameters, combined with the ReduceLRonPlateau dynamic learning rate adjustment method, default  $lr = 0.01$ , which reduced the learning rate to 10% (learning rate minimum  $10^{-5}$ ) of its original value if the validation loss did not decrease for three consecutive epochs (total 20 epochs). In the classical neural network, the FC1 layer has an output size of 50, while the output size of FC2 depends on the number of classes in the classification task. We used PennyLane[4] to construct and simulate the QCNN quantum layer, while PyTorch [26] served as the deep learning framework. All computations were simulated on CPU.

In the binary classification task, we selected all five subclasses from each superclass of the CIFAR-100 dataset, using a sliding window method to sequentially choose two classes to form the subdataset, resulting in four available datasets for each superclass.

Next, we conducted experiments on ten superclasses using the simplest QCNN circuit (without  $U_{OA}$ ), evaluating their performance in RGB, Lab, YCrCb, and HSV color spaces. Table 1 shows the highest classification accuracies for the corresponding tasks are presented. By comparing the experimental results across different color spaces, we observed that RGB maintained superior classification accuracy in most scenarios. Among the four color spaces, the subset  $\{caterpillar, cockroach\}$  of the Insects superclass achieved the best classification performance. The Lab color space achieved a test accuracy of 92.41% in this task, exceeding RGB.

Furthermore, we selected five superclasses that demonstrated balanced and outstanding performance across different color spaces, and tested these superclasses using circuits with enhanced entangling and expressive capabilities:  $U_{OA}(a)$  and  $U_{OA}(b)$ . As shown in Table 2, RGB performed best in the Fish and Fruit superclasses, with the quantum convolution circuit using  $CNOT$  achieving a maximum accuracy of 94.64% in the subset  $\{mushroom, orange\}$  of the Fruit superclass, representing a 7.6% improvement compared to the simplest circuit. The curve as shown Figure 6. For the binary classification results of the Vehicles2 superclass, it was evident that different classification scenarios benefited more from Lab, YCrCb, and HSV. In the  $\{tank, tractor\}$  subset (Vehicles2[3,4]), HSV outperformed RGB by 7% – 11%. In the Scenes[3,4] dataset, similar results were observed: HSV achieved an accuracy of 82.14%, while YCrCb reached 79.01%, both outperforming RGB. Additionally, the ablation study results demonstrated that using  $CRX$  for classification yielded higher accuracy than  $CNOT$  in some specific scenarios.

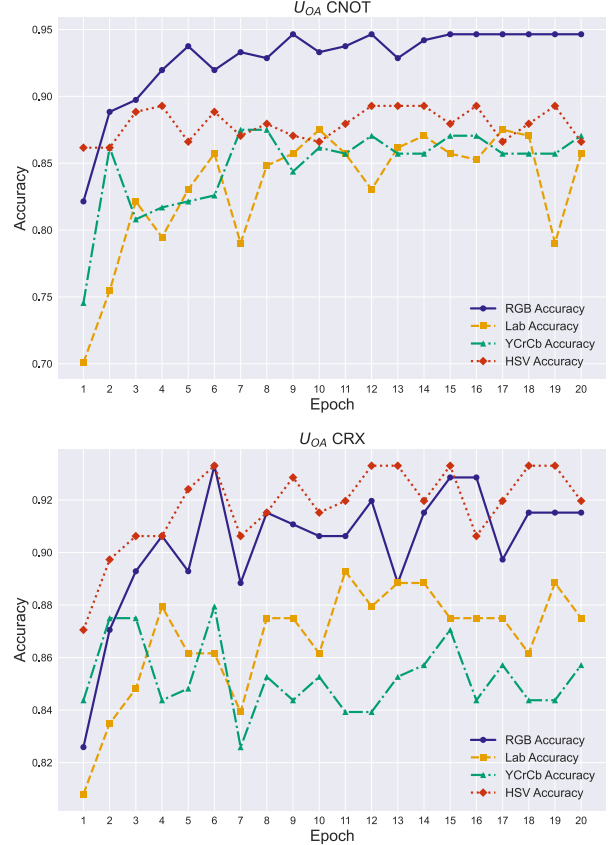


Figure 6. The classification accuracy curves for the Fruit[1,2] dataset are depicted, illustrating the performance under different  $U_{OA}$  configurations and color spaces.

## 5. Conclusion

In this work, we propose the HQCCNN model, which effectively classifies images across different color spaces for the CIFAR-100 dataset. By using the simplest QCNN structure (without  $U_{OA}$ ) for preliminary experiments, we observed that, aside from the RGB color space, other color spaces demonstrated more pronounced advantages in certain scenarios. After introducing the  $U_{OA}$  quantum fully connected layer, we compared the classification accuracy of two types of controlled rotation gates and examined different dataset types. The results indicate that, for the Fish and Fruit superclasses, RGB achieved the highest classification accuracy and demonstrated greater stability. However, results for the other three superclasses showed that RGB is not always the best choice, and different color spaces performed better in specific application scenarios.

Our research shows that the HQCCNN model we proposed, under reduced computational resource conditions, effectively identifies image categories with potential quantum advantages in computer vision tasks. This provides

an effective approach for exploring the strengths of hybrid quantum-classical systems. Additionally, different designs of PQC significantly impact feature performance, making the design of suitable PQCs for hybrid systems a crucial focus for future research.

In summary, our method identifies the performance of different image classification tasks and color spaces within such a hybrid quantum-classical system, thereby determining their potential to effectively leverage quantum advantage in specific application scenarios. We are confident that these results will provide valuable references and experimental insights for further exploration of models that utilize quantum computing advantages in color image classification within computer vision.

## References

- [1] Ryan Babbush, Jarrod R McClean, Michael Newman, Craig Gidney, Sergio Boixo, and Hartmut Neven. Focus beyond quadratic speedups for error-corrected quantum advantage. PRX quantum, 2(1):010103, 2021. 1
- [2] Adriano Barenco, Charles H Bennett, Richard Cleve, David P DiVincenzo, Norman Margolus, Peter Shor, Tycho Sleator, John A Smolin, and Harald Weinfurter. Elementary gates for quantum computation. Physical review A, 52(5):3457, 1995. 4
- [3] Marcello Benedetti, Erika Lloyd, Stefan Sack, and Mattia Fiorentini. Parameterized quantum circuits as machine learning models. Quantum Science and Technology, 4(4):043001, 2019. 2
- [4] Ville Bergholm, Josh Izaac, Maria Schuld, Christian Gogolin, Shahnawaz Ahmed, Vishnu Ajith, M Sohaib Alam, Guillermo Alonso-Linaje, B AkashNarayanan, Ali Asadi, et al. Pennylane: Automatic differentiation of hybrid quantum-classical computations. arXiv preprint arXiv:1811.04968, 2018. 7
- [5] Gary Bradski, Adrian Kaehler, et al. Opencv. Dr. Dobb's journal of software tools, 3(2), 2000. 6
- [6] Marco Cerezo, Akira Sone, Tyler Volkoff, Lukasz Cincio, and Patrick J Coles. Cost function dependent barren plateaus in shallow parametrized quantum circuits. Nature communications, 12(1):1791, 2021. 4
- [7] Andrew M Childs, Richard Cleve, Enrico Deotto, Edward Farhi, Sam Gutmann, and Daniel A Spielman. Exponential algorithmic speedup by a quantum walk. In Proceedings of the thirty-fifth annual ACM symposium on Theory of computing, pages 59–68, 2003. 1
- [8] Iris Cong, Soonwon Choi, and Mikhail D Lukin. Quantum convolutional neural networks. Nature Physics, 15(12):1273–1278, 2019. 1
- [9] Arturo De La Escalera, Luis E Moreno, Miguel Angel Salichs, and José María Armingol. Road traffic sign detection and classification. IEEE transactions on industrial electronics, 44(6):848–859, 1997. 1
- [10] Edward Farhi, Jeffrey Goldstone, and Sam Gutmann. A quantum approximate optimization algorithm. arXiv preprint arXiv:1411.4028, 2014. 2
- [11] Elies Gil-Fuster, Jens Eisert, and Carlos Bravo-Prieto. Understanding quantum machine learning also requires rethinking generalization. Nature Communications, 15(1):2277, 2024. 1, 2
- [12] Kaiming He, Xiangyu Zhang, Shaoqing Ren, and Jian Sun. Deep residual learning for image recognition. In Proceedings of the IEEE conference on computer vision and pattern recognition, pages 770–778, 2016. 1
- [13] Maxwell Henderson, Samridhi Shakya, Shashindra Pradhan, and Tristan Cook. Quantum convolutional neural networks: powering image recognition with quantum circuits. Quantum Machine Intelligence, 2(1):2, 2020. 3
- [14] Gao Huang, Zhuang Liu, Laurens Van Der Maaten, and Kilian Q Weinberger. Densely connected convolutional networks. In Proceedings of the IEEE conference on computer vision and pattern recognition, pages 4700–4708, 2017. 1
- [15] Yu Jing, Xiaogang Li, Yang Yang, Chonghang Wu, Wenbing Fu, Wei Hu, Yuanyuan Li, and Hua Xu. Rgb image classification with quantum convolutional ansatz. Quantum Information Processing, 21(3):101, 2022. 3
- [16] Richard Jozsa and Noah Linden. On the role of entanglement in quantum-computational speed-up. Proceedings of the Royal Society of London. Series A: Mathematical, Physical and Engineering Sciences, 459(2036):2011–2032, 2003. 1
- [17] Abhinav Kandala, Antonio Mezzacapo, Kristan Temme, Maika Takita, Markus Brink, Jerry M Chow, and Jay M Gambetta. Hardware-efficient variational quantum eigensolver for small molecules and quantum magnets. nature, 549(7671):242–246, 2017. 2
- [18] Morteza Khanramaki, Ezzatollah Askari Asli-Ardeh, and Ehsan Kozegar. Citrus pests classification using an ensemble of deep learning models. Computers and Electronics in Agriculture, 186:106192, 2021. 2
- [19] Ruba Kharsa, Ahmed Bouridane, and Abbes Amira. Advances in quantum machine learning and deep learning for image classification: a survey. Neurocomputing, 560:126843, 2023. 4
- [20] Korbinian Kottmann, Luis Mantilla Calderon, and Maurice Weber. Generalization in qml from few training data, 2024. Accessed: November 15, 2024. 4
- [21] Junhua Liu, Kwan Hui Lim, Kristin L Wood, Wei Huang, Chu Guo, and He-Liang Huang. Hybrid quantum-classical convolutional neural networks. Science China Physics, Mechanics & Astronomy, 64(9):290311, 2021. 3
- [22] I Loshchilov. Decoupled weight decay regularization. arXiv preprint arXiv:1711.05101, 2017. 7
- [23] Andrew L Maas, Awni Y Hannun, Andrew Y Ng, et al. Rectifier nonlinearities improve neural network acoustic models. In Proc. icml, page 3. Atlanta, GA, 2013. 5
- [24] Germano Moreira, Sandro Augusto Magalhães, Tatiana Pinho, Filipe Neves dos Santos, and Mário Cunha. Benchmark of deep learning and a proposed hsv colour space models for the detection and classification of greenhouse tomato. Agronomy, 12(2):356, 2022. 2
- [25] Emmanuel Ovalle-Magallanes, Dora E Alvarado-Carrillo, Juan Gabriel Avina-Cervantes, Ivan Cruz-Aceves, and Jose



- Ruiz-Pinales. Quantum angle encoding with learnable rotation applied to quantum-classical convolutional neural networks. Applied Soft Computing, 141:110307, 2023. 3
- [26] Adam Paszke, Sam Gross, Soumith Chintala, Gregory Chanan, Edward Yang, Zachary DeVito, Zeming Lin, Alban Desmaison, Luca Antiga, and Adam Lerer. Automatic differentiation in pytorch. 2017. 7
- [27] Ananda S Paymode and Vandana B Malode. Transfer learning for multi-crop leaf disease image classification using convolutional neural network vgg. Artificial Intelligence in Agriculture, 6:23–33, 2022. 1
- [28] F. Pedregosa, G. Varoquaux, A. Gramfort, V. Michel, B. Thirion, O. Grisel, M. Blondel, P. Prettenhofer, R. Weiss, V. Dubourg, J. Vanderplas, A. Passos, D. Cournapeau, M. Brucher, M. Perrot, and E. Duchesnay. Scikit-learn: Machine learning in Python. Journal of Machine Learning Research, 12:2825–2830, 2011. 7
- [29] Alberto Peruzzo, Jarrod McClean, Peter Shadbolt, Man-Hong Yung, Xiao-Qi Zhou, Peter J Love, Alán Aspuru-Guzik, and Jeremy L O’Brien. A variational eigenvalue solver on a photonic quantum processor. Nature communications, 5(1):4213, 2014. 2
- [30] Arthur Pesah, Marco Cerezo, Samson Wang, Tyler Volkoff, Andrew T Sornborger, and Patrick J Coles. Absence of barren plateaus in quantum convolutional neural networks. Physical Review X, 11(4):041011, 2021. 2
- [31] Tuan D Pham. A comprehensive study on classification of covid-19 on computed tomography with pretrained convolutional neural networks. Scientific reports, 10(1):16942, 2020. 1
- [32] Hanh Phan-Xuan, Thuong Le-Tien, Thuy Nguyen-Chinh, Thien Do-Tieu, Qui Nguyen-Van, and Tuan Nguyen-Thanh. Preserving spatial information to enhance performance of image forgery classification. In 2019 International Conference on Advanced Technologies for Communications (ATC), pages 50–55. IEEE, 2019. 2
- [33] Waseem Rawat and Zenghui Wang. Deep convolutional neural networks for image classification: A comprehensive review. Neural computation, 29(9):2352–2449, 2017. 1
- [34] Zhonghe Ren, Fengzhou Fang, Ning Yan, and You Wu. State of the art in defect detection based on machine vision. International Journal of Precision Engineering and Manufacturing-Green Technology, 9(2):661–691, 2022. 1
- [35] Farina Riaz, Shahab Abdulla, Hajime Suzuki, Srinjoy Ganguly, Ravinesh C Deo, and Susan Hopkins. Accurate image multi-class classification neural network model with quantum entanglement approach. Sensors, 23(5):2753, 2023. 3
- [36] David E Rumelhart, Geoffrey E Hinton, and Ronald J Williams. Learning internal representations by error propagation, parallel distributed processing, explorations in the microstructure of cognition, ed. de rumelhart and j. mccllland. vol. 1. 1986. Biometrika, 71(599-607):6, 1986. 5
- [37] Maria Schuld, Ilya Sinayskiy, and Francesco Petruccione. The quest for a quantum neural network. Quantum Information Processing, 13:2567–2586, 2014. 1
- [38] Arsenii Senokosov, Alexandr Sedykh, Asel Sagingalieva, Basil Kyriacou, and Alexey Melnikov. Quantum machine learning for image classification. Machine Learning: Science and Technology, 5(1):015040, 2024. 2, 4
- [39] Sukin Sim, Peter D Johnson, and Alán Aspuru-Guzik. Expressibility and entangling capability of parameterized quantum circuits for hybrid quantum-classical algorithms. Advanced Quantum Technologies, 2(12):1900070, 2019. 3, 5
- [40] Swarit Anand Singh and Kaushal A Desai. Automated surface defect detection framework using machine vision and convolutional neural networks. Journal of Intelligent Manufacturing, 34(4):1995–2011, 2023. 1
- [41] Anthony M Smaldone, Gregory W Kyro, and Victor S Batista. Quantum convolutional neural networks for multi-channel supervised learning. Quantum Machine Intelligence, 5(2):41, 2023. 3
- [42] QingZeng Song, Lei Zhao, XingKe Luo, and XueChen Dou. Using deep learning for classification of lung nodules on computed tomography images. Journal of healthcare engineering, 2017(1):8314740, 2017. 1
- [43] Tolga Turay and Tanya Vladimirova. Toward performing image classification and object detection with convolutional neural networks in autonomous driving systems: A survey. IEEE Access, 10:14076–14119, 2022. 1
- [44] Athanasios Voulodimos, Nikolaos Doulamis, Anastasios Doulamis, and Eftychios Protopapadakis. Deep learning for computer vision: A brief review. Computational intelligence and neuroscience, 2018(1):7068349, 2018. 1
- [45] Zhihui Wang, Stuart Hadfield, Zhang Jiang, and Eleanor G Rieffel. Quantum approximate optimization algorithm for maxcut: A fermionic view. Physical Review A, 97(2):022304, 2018. 2
- [46] Ronald J Williams and David Zipser. A learning algorithm for continually running fully recurrent neural networks. Neural computation, 1(2):270–280, 1989. 5
- [47] Ming Yang, Pawan Kumar, Jyoti Bhola, and Mohammad Shabaz. Development of image recognition software based on artificial intelligence algorithm for the efficient sorting of apple fruit. International Journal of System Assurance Engineering and Management, 13(Suppl 1):322–330, 2022. 1
- [48] Yuan-Fu Yang and Min Sun. Semiconductor defect detection by hybrid classical-quantum deep learning. In Proceedings of the IEEE/CVF Conference on Computer Vision and Pattern Recognition, pages 2323–2332, 2022. 3